Radiometric and Spectral Characteristics of the ScaRaB-3 Instrument on Megha-Tropiques: Comparisons with ERBE, CERES, and GERB

Michel Viollier, Patrick Raberanto

Radiometric and Spectral Characteristics of the ScaRaB-3 Instrument on Megha-Tropiques: Comparisons with ERBE, CERES, and GERB

MICHEL VIOLLIER* AND PATRICK RABERANTO

Laboratoire de Météorologie Dynamique/IPSL/CNRS, Ecole Polytechnique, Palaiseau, France

(Manuscript received 16 March 2009, in final form 7 September 2009)

ABSTRACT

The Indian–French Megha-Tropiques mission, scheduled to be launched in 2010, will carry radiation and microwave sensors to study the energy and water cycle in the tropics. The radiation sensor, the third model of the Scanner for Radiation Budget (ScaRaB-3), is dedicated to the earth's radiation budget, the difference between the solar absorbed flux and the terrestrial emitted flux. These fluxes are calculated from satellite measurements of outgoing shortwave (SW) and longwave (LW) radiances using angular distribution models (ADMs). For practical reasons, the LW radiation is calculated from the difference between a total (T) channel (0.2–100 μm) and an SW channel (0.2–4 μm). With the ADM application, the radiance calibration remains the most critical issue in the radiation budget estimation. The 1% accuracy goal is difficult to achieve, specifically in the SW domain. The authors explain their efforts to improve the radiometric calibration of ScaRaB-3. The internal calibration module is improved: the sensor is switched between SW and T channels by rotating the filter wheel on which the SW filter is now installed. Because the pyroelectric detector is sensitive to the thermal effect of the electromagnetic radiation independently of its spectral range, this plan allows calibrating the SW channel as a T channel by viewing a blackbody. Indeed, the transfer of the T calibration to the SW domain requires perfect knowledge of the total spectral response and of the transmittance of the SW filter, which is discussed in the article. Spectral errors are calculated with updated data. In the SW domain, they are found to be the smallest compared to those of the Earth Radiation Budget Experiment (ERBE), the Clouds and the Earth's Radiant Energy System (CERES), and the Geostationary Earth Radiation Budget (GERB).

1. Introduction

Earth radiation budget (ERB) data have been provided for the last decades effectively by two National Aeronautics and Space Administration (NASA) missions: the Earth Radiation Budget Experiment (ERBE; Barkstrom et al. 1989) and the Clouds and the Earth's Radiant Energy System (CERES; Wielicki et al. 1996). This series has been completed by the Scanner for Radiation Budget (ScaRaB) instrument designed at the Laboratoire de Météorologie Dynamique (LMD; Monge et al. 1991; Kandel et al. 1998). Two models of this instrument were launched into space in January 1994 (Kandel et al. 1998) and in August 1998 (Duvel et al. 2001). The third series of ERB instrument is the Geostationary Earth Radiation Budget (GERB; Harries et al. 2005), which provides ERB estimates from the geostationary satellites *Meteosat-8* and *Meteosat-9* since 2003. In the future, the broadband radiometer (BBR) will complete the payload of the European Space Agency/Japan Aerospace Exploration Agency (ESA/JAXA) Earth, Clouds, Aerosols and Radiation Explorer (EarthCARE) mission (Gelsthorpe et al. 2008). Together with the application of the angular distribution models (ADMs), the radiometric calibration remains the most critical issue for all these missions (for the impact on the global estimates, see Loeb et al. 2009). The 1% accuracy goal is difficult to achieve, specifically in the shortwave (SW) domain. Because a third model of ScaRaB is now planned to be launched in 2010 on the French–Indian Megha-Tropiques (MT) mission, we explain in this paper our efforts for improving the radiometric calibration of this new instrument, which we compare with the other ERB instruments.

More generally, absolute accuracy is a crucial issue in the use of satellite data for climate and environment studies. Whatever complex algorithms or simple threshold

* Deceased.

Corresponding author address: Patrick Raberanto, Laboratoire de Météorologie Dynamique/IPSL/CNRS, Ecole Polytechnique, 91128 Palaiseau, France.
E-mail: raberanto@lmd.polytechnique.fr

DOI: 10.1175/2009JTECHA1307.1

techniques are used, the remote sensing results will mainly depend on the radiometric calibration. The variations in the calibration gains are particularly problematic in that these gain variations can be misinterpreted as trends in the atmospheric or surface properties. Improving the calibration of ERB instruments then contributes to a general effort for improving the quality of the remote sensing data products obtained from space. Beyond this trend detection issue, absolute radiometric calibration is also crucial for the validation of models of atmospheric radiation transfer or meteorological thermodynamic processes, where comparisons of energy estimates from different sources and nature are required. In the early ages of satellite remote sensing, vicarious calibration was used to correct the errors or absence of real calibration: for example, Viollier (1982) for Coastal Zone Color Scanner (CZCS)/*Nimbus-7* and Koepke (1982) for Meteosat. The principle is to substitute the internal calibration sources by terrestrial targets with characteristics assumed stable over time or being known with precision (from additional atmospheric and surface measurement). Among these targets, the most used for the solar domain are the deserts [used for Systeme pour l'Observation de la Terre (SPOT) and Meteosat] and atmospheric Rayleigh scattering [Polarization and Directionality of the Earth Reflectances (POLDER) and ocean color sensors]. For climate applications, the use of these methods cannot be absolutely recommended, because the stability of ground targets may itself be affected by climate change through changes in surface properties or the atmosphere. However, as illustrated by the 2% agreement between POLDER and CERES SW reflected fluxes (Buriez et al. 2007), comparison between vicarious and absolute calibration methods remains a powerful validation tool. Hu et al. (2004) recently have reexamined this approach, recommending using the ''deep convective clouds'' (DCC) as a substitute for the CERES SW calibration source. From discussion on the ScaRaB-3 calibration, this paper will cover these different topics. First, it recalls the main principles of ERB calibration (section 2) and the characteristics of the main ERB instruments (section 3). The new radiometric and spectral characterizations of ScaRaB-3 are then presented and compared to the ERB instruments (section 4). The different steps of the ScaRaB-3 calibration are described in section 5, and the auxiliary vicarious methods are described in section 6. The calibration strategy is summarized in section 7.

2. Main principles of ERB calibration

All ERB missions since ERBE are based on broadband radiometers that measure the SW reflected solar radiation (0.2–4 μm) and the longwave (LW) emitted terrestrial radiation (4–100 μm) with high absolute accuracy (1%–2%) because of onboard calibration modules (blackbody, lamps, and solar diffuser) and careful calibration analyses. In fact, the LW radiation is obtained from the subtraction between a total (T) channel (0.2–100 μm) and an SW channel (0.2–4 μm). Beside these two main channels, ERBE had an LW channel (6–35 μm), which was replaced for CERES by an infrared window channel (8–12 μm). ScaRaB has two auxiliary channels, a visible (VIS) channel (0.55–0.65 μm) and an infrared window channel (10.5–12.5 μm) for scene identification and for facilitating combination with narrowband data from geostationary meteorological satellites.

The responses of both main channels should be as flat as possible. In reality, they cannot be perfectly flat because of the physical properties of the components (detectors, mirrors, and filters), and they are characterized by spectral response functions. The instruments then do not measure a real radiance but a filtered radiance. For each channel k (SW or T), this quantity is defined by

$$L_K^f = \int_0^\infty L(\lambda) r_K(\lambda)\, d\lambda, \tag{1}$$

where $L(\lambda)$ is the radiance of the observed scene or calibration source at wavelength λ and $r_k(\lambda)$ is the spectral response functions of channel k. The spectral response functions are relative values and may be scaled in different ways: value of 1 at maximum or any other normalization method.

Assuming response linearity, the radiometric calibration is the calculation of the gain G_k for each channel k:

$$G_K = \frac{N_K}{L_K^f}, \tag{2}$$

where N_k is the instrument output (scene signal subtracted from the space signal) and L_k^f is the filtered radiance. According to Eq. (1), L_k^f depends on the spectrum of the scene being observed (ocean, land, clouds, various cloud, and surface combination) or of the calibration source. Therefore, L_k^f must refer to a well-specified spectral response [i.e., a reference spectral target of radiance $L_{\text{ref}}(\lambda)$]. The case of any other spectral response has to be adjusted by a spectral correction. This correction is done at the level-2 data processing stage because scene identification is normally required in these calculations. Indeed the real (unfiltered) radiance L is deduced from the filtered radiance L^f and from predetermined filtering factors F_{scene},

$$L = \frac{L^f}{F_{\text{scene}}}, \tag{3}$$

where F_{scene} is estimated from the spectral radiances $L_{\text{scene}}(\lambda)$ of different scenes:

$$F_{\text{scene}} = \frac{\int_0^\infty L_{\text{scene}}(\lambda) r_K(\lambda)\, d\lambda}{\int_0^\infty L_{\text{scene}}(\lambda)\, d\lambda}. \tag{4}$$

Here F_{scene} is equal to 1 if $L_{\text{scene}}(\lambda)$ has the same spectral response as the reference source [i.e., if $L_{\text{scene}}(\lambda)$ is proportional to $L_{\text{ref}}(\lambda)$]. Note that F_{scene} also depends implicitly on the viewing geometry. Because the spectral responses are relatively flat, the correction remains small. For ScaRaB-1 and ScaRaB-2, the peak-to-peak range of variation of F_{scene} was within $\pm 3\%$ for the SW domain. The rms error after corrections was estimated as 0.88%. This marks the difference with ERB estimates from narrowband instruments, for which the spectral corrections would be much larger [see section 5d(3)].

From Eqs. (1) and (2), it is clear that G depends on the normalization of $r_k(\lambda)$. Indeed, $r_k(\lambda)$ can be scaled according to different definitions: $r_k(\lambda) = 1$ at maximum; $r_k(\lambda)$ derived from the raw spectral measurements; and $r_k(\lambda)$ normalized such that the spectral integral is equal to a given constant. However, the influence of the r normalization is removed when the filtering factor is calculated [Eq. (4)]. This condition requires an excellent agreement between the level-1 and level-2 data processing systems: the same normalized spectral response $r_k(\lambda)$ must be used both in the computation of G [Eqs. (1) and (2) at level 1] and in the computation of the filtering factors and unfiltered radiances [Eqs. (3) and (4) at level 2]. The ERBE and CERES data processing do not use the same formalism. However, the rationale (Loeb et al. 2001) is identical: from a set of modeled spectral distributions of the earth's radiation, the relationship between the filtered radiance [calculated with $0 < r(\lambda) < 1$] and the filtered radiances is estimated and applied.

3. ERB instruments and their calibration

a. CERES

The CERES instrument design is basically the same as the ERBE instrument (Barkstrom et al. 1989). Three radiometric channels are coaligned and mounted on a rotating axis that scans the earth from horizon to horizon and the calibration sources. The three sensors cover the SW, total, and infrared window domains. The infrared window channel (8–12 μm) has replaced the imperfect ERBE LW channel (6–35 μm). Each sensor is based on a thermistor bolometer detector comprised of active and reference discs, Cassegrain optics, and filters. For the SW channel, the filter is a 1-mm-thick fused, waterless quartz element (SiO_2). The detectors are covered with a black paint layer, which absorbs the input radiation and causes a measurable change in temperature. Contrary to ERBE, ScaRaB, and GERB, the telescope mirrors are coated with silver instead of aluminum to improve the flatness of the spectral response (see section 4b). To improve the ADM knowledge, two identical instruments are aboard both satellites *Terra* [flight model 1 (FM1) and FM2] and *Aqua* (FM3 and FM4). Alternatively, each instrument works in across-track or rotating-azimuth plane mode. Priestley et al. (2000, 2002) have described the internal calibration module (ICM) based on blackbodies, tungsten lamps [SW internal calibration source (SWICS)], and solar diffuser [mirror attenuator mosaic (MAM)]. For the SW calibration, the solar diffuser sources or MAM showed large anomalous trends and were considered useless. However, the estimations of SW gains based on calibration lamps were found extremely stable over several years. However, by comparing the instantaneous measurements from two instruments, anomalies greater than 1% were found (Matthews et al. 2005) and attributed to filter degradation. The darkening of the spectral response is explained by the fixation of contaminants to optical surfaces when they are directly exposed to solar incidence (in rotating-azimuth plane mode). These degradations occurred at the shortest wavelengths, outside the lamp spectral emission, and they could not be corrected by the lamp calibration system. Corrections have been applied, but the CERES calibration analysis outlines the extreme difficulty of the SW calibration.

b. ScaRaB-1 and ScaRaB-2

The instrument has been described in depth by Monge et al. (1991) and Kandel et al. (1994). ScaRaB is a four-channel cross-track scanning radiometer (Table 1). In addition to the main channels, ScaRaB has two auxiliary channels, a visible channel (0.55–0.65 μm) and an infrared window channel (10.5–12.5 μm) for scene identification and for facilitating combination with meteorological geostationary sensors. The earth-scanning angle is 100°. Scanning is obtained by rotation of a cylinder (rotor, Fig. 1) carrying the optics, filters, detectors, choppers, and analog–digital conversion electronics around an axis parallel to the spacecraft velocity vector and within a cylinder (stator) mounted on the spacecraft. The four parallel telescopes focus the incoming radiation on four

TABLE 1. ScaRaB channels.

Channel No.	Description	Wavelength range	Filter type
1	VIS	0.55–0.65 μm	Interference
2	Solar (SW)	0.2–4 μm	Fused silica
3	T	0.2–50 μm	Unfiltered
4	IRW	10.5–12.5 μm	Interference

pyroelectric detectors ($LiTO_3$ crystal) coated with black paint and located at the prime focus of a spherical aluminum mirror. The pyroelectric detectors are more sensitive than the CERES bolometers but less stable in time. The high sensitivity allows simplifying the optics (one-mirror telescope). But the lack of stability requires a quasi-permanent comparison with a stable source obtained by modulated detection. Indeed, two mechanical choppers (16 Hz) have been implemented, one for channels 1 and 2 and one for channels 3 and 4, consisting of a hemispherical mirror fitted with two apertures. The radiance measurement is given by the difference between the signal coming from the scene (16 samples; i.e., 16 ms) and the signal coming from a reference internal blackbody. Note that because the filters used for channels 1, 2, and 4 are located between the chopper and the detector, their thermal emission is eliminated. This scene signal is referred to the zero radiance level because of the space view (375 ms) each scan period. The raw instrument output [N_k of Eq. (2)] is then computed from the difference of the scene and space measurements. Finally, absolute calibration is achieved from the observation of internal sources.

Radiometric performances of ScaRaB-1 and ScaRaB-2 were estimated on the ground (Sirou et al. 1997). In a vacuum chamber, ScaRaB was characterized with an actively controlled-temperature blackbody. These operations established the linearity of response and provided radiometric calibration of the temperature and emissivity of the onboard calibration blackbodies and calibration of the temperature dependence of detector gains. Onboard shortwave sources were calibrated at high-altitude sites (Mueller et al. 1997) against a sun-illuminated diffuser with incoming solar flux measured by high-standard calibrated pyrheliometer and in the laboratory against calibrated integrating sphere.

In flight, the temperature of the reference blackbody for channel 3 is measured by a thermometric sonde and included in the scientific telemetry. For the SW domain, the calibration system was designed with three sets of preaged incandescent lamp sources (Trémas and Dinguirard 1997). The channel stability (or, more exactly, the temperature-gain function) was measured in flight on channel 3 and reached an excellent value of 0.1% (Duvel and Raberanto 2000). Intercomparisons between ScaRaB and ERBE wide field of view (Bess et al. 1997) and between ScaRaB and CERES (Haeffelin et al. 2001) also have been carried out. According to the results of all these operations, the observed radiance differences were estimated to be 1% in the longwave and 2% in the shortwave domains.

c. *ScaRaB-3 on Megha-Tropiques*

A third ScaRaB instrument is being tested for implementation on the Megha-Tropiques mission (a joint science project between India and France). The main objective of this mission is to study the energy and hydrological cycles in the tropics. The launch is planned for 2010. At an altitude of 867 km, the satellite will be placed in an orbit of low inclination (20° to the equator)

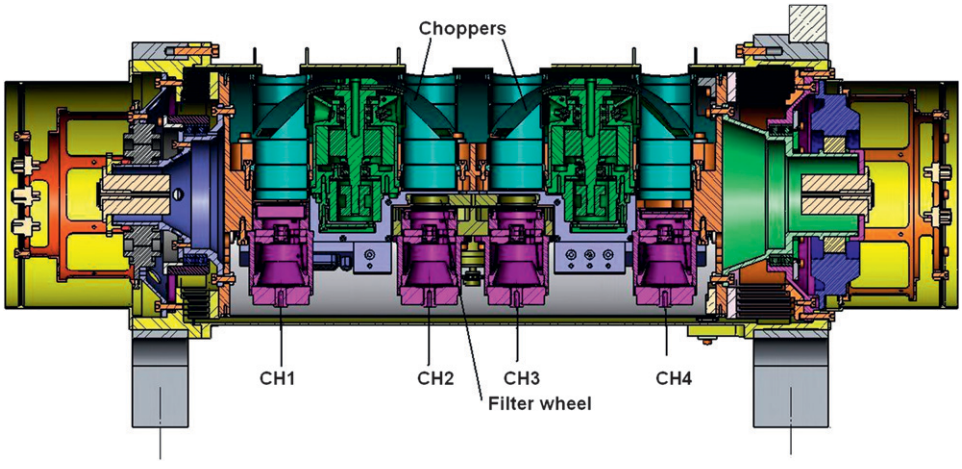

FIG. 1. The ScaRaB rotor. The instrument is organized around two choppers, one for channels 1 (VIS) and 2 (SW) and the other for channels 3 (T) and 4 (IRW).

to obtain the best time sampling in the tropical zone (30°S–30°N). The other payloads are microwave radiometers and humidity sounders. Although based on the spare model of the preceding missions, the Megha-Tropiques ScaRaB instrument can be considered as entirely new, because most of the components (detectors, optics, mechanisms, and electronics) have been updated. But the general concept is unchanged. The only major change concerns the calibration onboard procedure, which benefits from the experience feedbacks of the two preceding ScaRaB experiences and of the other ERB experiments (ERBE, CERES, and GERB). The SW filter is now removable, which allows calibrating channel 2 by viewing a blackbody. With this concept, the use of imperfect SW sources (lamps or solar diffuser) is avoided. Because the pyroelectric detector is sensitive to the thermal effect of the electromagnetic radiation independent of its spectral range, the SW calibration can be transferred from the LW domain. Obviously, this assumes that the total spectral response and the transmittance of the SW filter are perfectly known and stable. The SW filter is removable, because it is now implemented on a filter wheel (Fig. 2). Because of this new design, there are three in-flight calibration modes:

1) Calibration mode (C mode): The purpose of this mode is to check gain stability of all the channels using internal blackbodies and lamp (channel 1). In this mode, the filter wheel is activated to have no filter in front of channels 2 and 3.
2) Total mode (T mode): In this mode, the filter wheel is activated to place no filter on channels 2 and 3. The purpose of this calibration mode is to compare measurements from geophysical scenes obtained from channels 2 and 3 as total channels.
3) Solar mode (S mode): In this mode, the filter wheel is activated to place identical solar filters on channels 2 and 3. The purpose of this calibration mode is to compare measurements from geophysical scenes obtained from channels 2 and 3 as solar channels.

For ERB estimation, the measurement mode (M mode) is used with solar filter on channel 2 (SW radiation) and no filter on channel 3 (Total radiation).

d. GERB

The first GERB was launched on board *Meteosat-8* in August 2002, and the second was launched on board *Meteosat-9* in December 2005. Since the beginning of data transmission in December 2002, these instruments have provided fields of SW and LW radiances over the Meteosat disc centered at 0° longitude each 15 min (Harries et al. 2005). GERB uses a despin mechanism to counteract the Meteosat spacecraft rotation, making instrument design rather complex. The present simplified summary focuses on calibration issues. Indeed, GERB has only one telescope, and the 256 × 256 element field is generated with a linear 256-element detector array (north–south direction) and by sampling over the spacecraft rotation (east–west direction). The telescope is equivalent to a total channel. The SW channel results from alternative scans with the telescope covered by a quartz SW filter. A full earth disc is acquired in 6 min. Although pairs of total and SW scans may be separated in time by up to 6 min, the GERB design has the advantage of using a single telescope for both spectral bands. In flight, the total channel is calibrated using blackbodies and space views. One difficulty arises from the validation of a large number of detectors (256). To monitor spectral response change in the SW channel, GERB observes an integrating sphere illuminated at certain periods by the sun. Spectral corrections are described by Clerbaux et al. (2008a,b). According to Dewitte et al. (2008) and for GERB-2 Edition 1 products, there is a GERB–CERES agreement within 5% and 2% for the SW and LW radiances, respectively. The main limit of accuracy of this product is assumed to lie in the knowledge of the SW response.

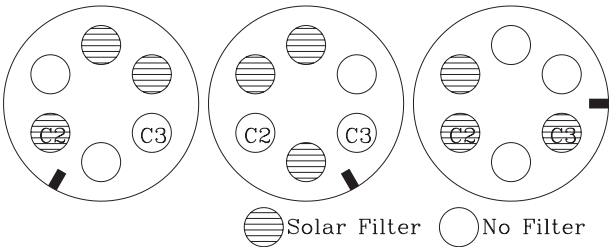

FIG. 2. The filter wheel allows three modes: (left) measurement mode M: solar filter on channel 2, no filter on channel 3; (middle) total T mode: no filter on both channels; and (right) solar S mode: solar filter on both channels. The T mode allows the calibration on internal sources (C Mode) and the comparison of both channels over terrestrial scenes. The S mode allows comparing the SW response of both channels on the earth's views.

4. Spectral and radiometric main characteristics of ScaRaB-3

a. Spectral response of total channels

Because the detectors and telescope mirrors of ScaRaB-3 are new, their spectral responses have been reexamined and compared to those of previous instruments. The spectral responses are measured using a monochromatic radiation from a visible or infrared source (quartz-halogen lamp and globar) successively recorded by each ScaRaB channel (the whole detector and

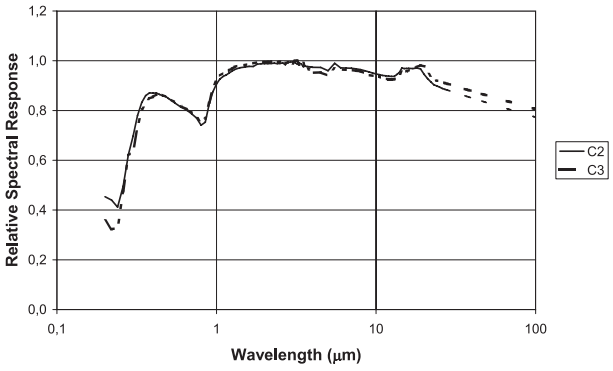

FIG. 3. Relative spectral responses of total channels 2 and 3 of ScaRaB-3/MT.

optic module) and by a pyroelectric cavity. The ratio of the measurements successively done by the channel and cavity provides the relative value of the spectral response. For most SW wavelengths (0.5–3 μm), the accuracy is excellent (better than 1%). However, beyond 6 μm, the signal coming from the monochromator becomes weak, so that a set of bandpass filters is used in addition. However, from 20 μm, the uncertainty becomes larger and larger, and the spectral behavior is completed with information coming from the detector constructors. The uncertainty at the largest wavelengths is estimated to be 15%. The impact on the calibration will be studied further [section 5b(3)]. Figure 3 shows the spectral responses of total channels 2 and 3 of ScaRaB-3/MT measured by this method. Fundamental for the instrument objectives, spectra are quasi-identical for channels 2 and 3. It is difficult to attribute the small differences to reality or to experimental errors. Figure 4 shows the comparison with the other ERB instruments. All the responses are relatively flat between 1 and 20 μm. From 0.2 to 1 μm, dispersion is large, which is reflected in the SW domain and discussed in the next section.

b. Spectral response of SW channel

In the new configuration, the SW channel corresponds to the channel 2 attenuated by the SW filter of the filter wheel in mode M (Fig. 2). The SW filter is a synthetic quartz glass also called fused silica (thickness of 10 mm). Our hypothesis is that the relative SW response is the product of the total response multiplied by the spectral transmittance of the filter. The spectral transmittance of the filter is shown in Fig. 5, measured at the Laboratoire National de Métrologie et d'Essais (F78, Trappes) with an accuracy of $\pm$0.7% between 0.2 and 2 μm and $\pm$1.0% between 2 and 4 μm. Note that a quartz filter usually transmits also beyond 40 μm, but with no significant consequence (see in section 5e). The three quartz filters of the filter wheel showed identical spectral transmittances ranged from 0.930 to 0.940 between 0.5 and 3.4 μm. The filter transmission results mainly from the reflection at the interfaces, and theoretical calculation with optical index of 1.4623 at 0.5 μm indicates about the same results (0.9307). By spectral integration with a 5800-K blackbody spectral distribution, the effective transmittance is estimated to be 0.931 in the range 0.2–4 μm (0.924 in the range 0.2–10 μm). The combination

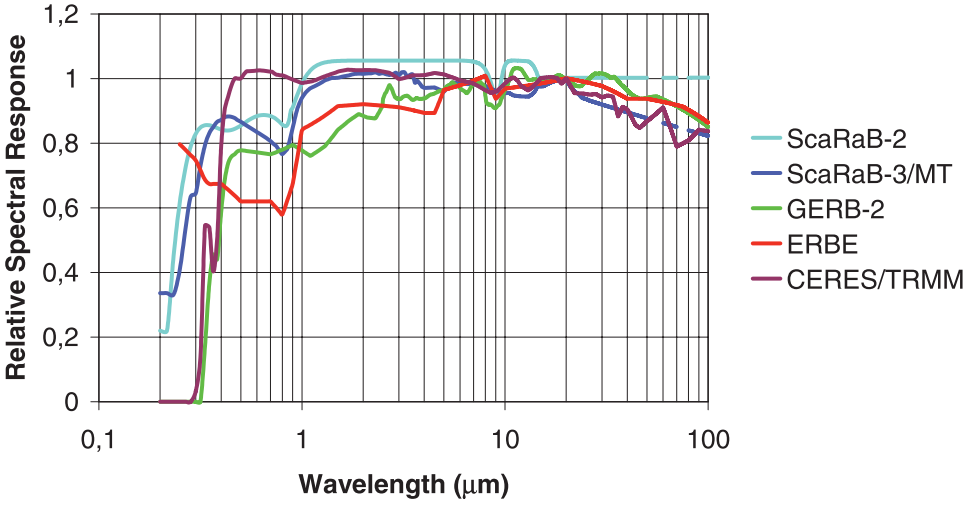

FIG. 4. Relative spectral responses of total channel of ScaRaB-3/MT (blue), and comparison with those of ScaRaB-2 (light blue), GERB-2 (green), ERBE (red) and CERES (purple). All are normalized to 1 at 20 μm. The data are from the GERB Web site (available online at http://ggsps.rl.ac.uk/information.html#Spectral) for GERB and Loeb et al. (2001) for CERES.

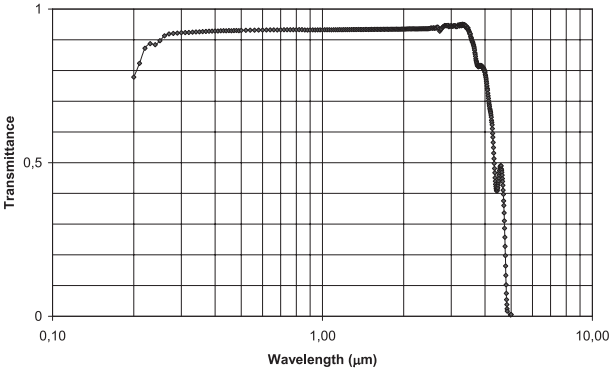

FIG. 5. Spectral transmittance of the quartz filter.

of the quartz spectral transmittance (Fig. 5) and of the channel 2 total spectral response gives the relative spectral responses of SW channel of ScaRaB-3/MT; it is shown in Fig. 6, with those of ScaRaB-2, GERB-2, ERBE, and CERES for comparison. Note that the silver-coated mirror used in CERES improves the flatness between 0.4 and 4 μm but cuts radiation below 0.35 μm. GERB also cuts the shortest wavelengths, and this is probably due to the successive attenuations by five mirrors. ScaRaB and ERBE have the largest responses at the shortest wavelengths, which leads to minimize the spectral corrections (Table 2).

c. *Blackbodies of the calibration module*

Precision blackbodies cannot be used on board because of their weight and volume. Simulators are used instead. For ScaRaB-1 and ScaRaB-2, the blackbody simulators developed by the Russian teams had an excellent emissivity of 0.993. For ScaRaB-3, we have developed new simulators. The ScaRaB-3 blackbodies have eight aluminum rings, and the diameter of the largest ring is 35 mm. The internal geometry has been studied to trap radiation by successive reflections. The rings are coated with black paint. The maximum mass of these blackbodies is 80 g. According to measurements carried out at Laboratoire National de Métrologie et d'Essais (F78, Trappes) the emissivity of the three new blackbodies was estimated to be 0.997 ($\pm$0.002) between 2 and 14 μm from measurements of their directional reflection factor. No significant differences were observed between the three blackbodies.

5. Gain estimation and spectral corrections for ScaRaB-3/MT

a. *Temperature dependence of gain*

All gain determinations described in the following sections are defined for a given instrument temperature T_m. During calibration phases, given T_c the instrument temperature, the estimated gain will be $G_k(T_c)$. During the measurement mode, if the instrument temperature moves to T_m, then the gain will be

$$G(T_m) = G(T_c)[1 + \alpha(T_m - T_c)]. \quad (5)$$

The Meteor measurements have demonstrated this linear temperature dependence on the level of about 0.1% for the four channels over a temperature range of 280–305 K (7°–32°C). For ScaRaB-3 Megha-Tropiques, thermal models predict a small range of variation (291–295 K,

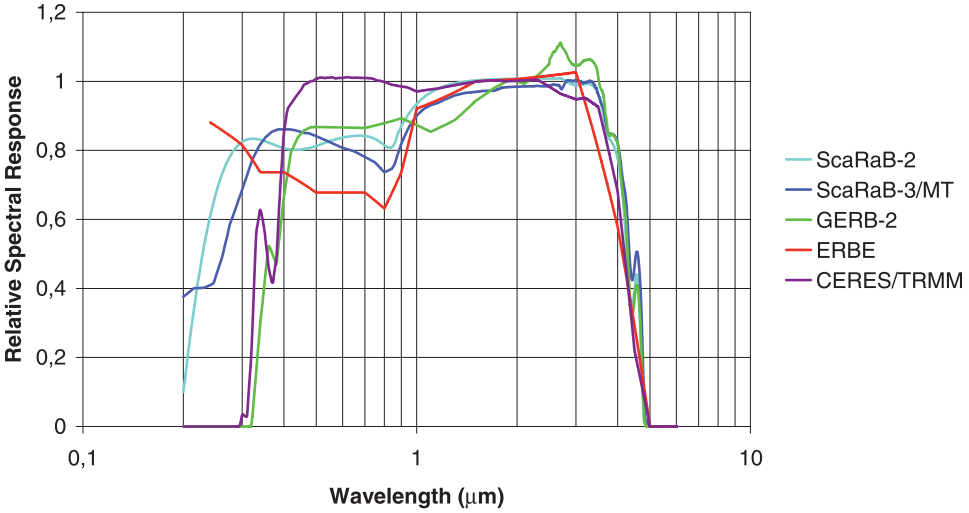

FIG. 6. As in Fig. 4, but for the SW channels. All are normalized to 1 at 2 μm. ERBE (red), ScaRaB-2 (blue), ScaRaB-3 (light blue), CERES (purple), GERB (green). The data sources are as in Fig. 4.

TABLE 2. Range of SW filtering factors and spectral errors for ScaRaB-3 and comparisons with other ERB instruments. The last line gives the equivalent for a narrow band in the visible (0.5–0.7 μm). For making the comparison significant, the same input dataset of the earth's spectral signatures have been used and the instrument spectral responses have been normalized in the same way (filtering factor equal to 1 for a blackbody at 5800 K). Earth Radiation Budget Satellite (ERBS).

	Filtering factor × 100		Spectral errors (W m^{-2} sr^{-1})	
	max–min	rms	max–min	rms
ScaRaB-1	8.02	1.54	9.95	1.54
ScaRaB-2	6.43	1.03	7.28	1.03
ScaRaB-3	2.74	0.46	3.23	0.62
ERBE/ERBS	9.64	1.53	10.02	1.93
CERES/TRMM	11.08	1.73	19.77	4.23
GERB-2	15.19	2.48	22.58	3.94
VIS narrow band	93.29	16.32	117.78	22.20

or 18°–22°C) so that the gain estimation will be less sensitive to this aspect. For simplification, the temperature dependence is removed from the following equations.

b. Normalization of spectral responses

The spectral responses of each channel have relative values and generally are normalized to be equal to 1 at their maximum value. For ScaRaB-1 and -2, Viollier et al. (1995) use the following formulas to normalize $r_T(\lambda)$ and $r_{SW}(\lambda)$:

$$\frac{\int_0^\infty B(\lambda, 310) r_T(\lambda)\, d\lambda}{\int_0^\infty B(\lambda, 310)\, d\lambda} = 1 \quad \text{and} \tag{6}$$

$$\frac{\int_0^\infty B(\lambda, 5800) r_{SW}(\lambda)\, d\lambda}{\int_0^\infty B(\lambda, 5800)\, d\lambda} = 1, \tag{7}$$

where $B(\lambda, 310)$ and $B(\lambda, 5800)$ are the blackbody spectral radiances for 310 and 5800 K, respectively. A temperature of 310 K was chosen as the temperature of calibration blackbody for ScaRaB-1 and ScaRaB-2. The advantage of this normalization is that the unfiltered and filtered radiances are identical when the instrument observes such blackbodies with spectral shape reasonably close to emitted and reflected solar SW radiance earth scenes. Then the range of filtering factors [Eq. (4)] is close to 1. For ScaRaB-3 with the removable SW filter, the normalization can be based only on the 310-K blackbody for the channel without filter, and the final spectral response will then be the 310-K normalized response multiplied by the filter transmittance. Such is the option taken for GERB for which the SW filter is also removable.

c. The nighttime LW case

This nighttime LW case is the simplest. For the earth's observation, the total radiance is measured by channel 3. This channel is calibrated through the C mode when it observes the blackbody simulator (BBS3) of the calibration module (CALM). The temperature of the blackbody T_{BBS3} is floating (no active thermal control) with a maximum variation range between 291 and 295 K (18°–22°C), close to the instrument temperature. This temperature is measured by a thermometric sonde and transferred to the telemetry. From the Stefan–Boltzmann law, the radiance of the blackbody simulators is accurately derived from the T_{BBS3} assuming the emissivity equal to 1:

$$L_{BBS3} = \frac{(\sigma T_{BBS3}^4)}{\pi}, \tag{8}$$

where σ is the Boltzmann constant (5.670×10^{-8} W m^{-2} K^{-4}).

1) BLACKBODY EMISSIVITY IMPACT

If we consider the real value of the emissivity ε slightly different from 1, the blackbody has a reflectivity of $1 - \varepsilon$ and then reflects the environment radiance. Consequently, the radiance of the blackbody is the sum of its own emission and of the reflected radiance of the environment. Equation (8) then becomes

$$L_{BBS3} = \frac{(\varepsilon\sigma T_{BBS3}^4 + (1-\varepsilon)\varepsilon_{env}\sigma T_{env}^4)}{\pi}, \tag{9}$$

where T_{env} and ε_{env} are the temperature and emissivity of the channel environment. Note that, if T_{BBS3} is equal to T_{env} and ε_{env} is close to 1, the emission and reflection errors mostly cancel each other and Eqs. (8) and (9) become equivalent. For ScaRaB-3, T_{BBS3} and T_{env} are close, because BBS3 has no active thermal control, and

then T_{BBS3} follows the instrument temperature variations. In such conditions and because the emissivity of the ScaRaB blackbodies is close to 1 (section 4c), the difference in using Eq. (8) instead of Eq. (9) is negligible. Simple calculation yields 0.25% difference in an improbable extreme case ($T_{env} = 293$ K, T_{BBS3} from 278 to 308 K, and $\varepsilon_{env} = 0.9$). The approximation in using $\varepsilon = 1$ then is valid, and Eq. (8) can then be employed for the calculation of L_{BBS3}.

2) LW SPECTRAL IMPACTS

Consider now the gain calculation and the impact of the channel spectral response. From the C calibration mode and according to Eq. (2), the gain G_3 can then be easily calculated:

$$G_3 = \frac{N_3}{L^f_{BBS3}}, \tag{10}$$

where N_3 is the raw instrument output for the C mode and L^f_{BBS3} is the filtered radiance of the blackbody simulator BBS3:

$$L^f_{BBS3} = \int_0^\infty L_{BBS3}(\lambda, T_{BBS3}) r_3(\lambda)\, d\lambda \tag{11}$$

The spectral radiance $L_{BBS3}(\lambda, T_{BBS3})$ is calculated from the Planck law. For ScaRaB-1 and ScaRaB-2, $r_3(\lambda)$ was rather constant in the infrared range, and then L^f_{BBS3} was equal to σT^4_{BBS3} [Eq. (8)] with almost negligible correction. If $r_3(\lambda)$ is not constant, the filtered radiance L^f_{BBS3} is deduced from the blackbody radiance L_{BBS3} with

$$L^f_{BBS3} = L_{BBS3} F_3(T_{BBS3}), \tag{12}$$

where $F_3(T_{BBS3})$ is the filtering factor and is estimated from the spectral radiances $L_{BBS3}(\lambda, T_{BBS3})$ of blackbody at temperature T_{BBS3},

$$F_3(T_{BBS3}) = \frac{\int_0^\infty L_{BBS3}(\lambda, T_{BBS3}) r_3(\lambda)\, d\lambda}{\int_0^\infty L_{BBS3}(\lambda, T_{BBS3})\, d\lambda}. \tag{13}$$

In conclusion, the gain G_3 is directly calculated within the C mode using Eq. (10) with L^f_{BBS3} calculated from the Boltzmann constant and the measured temperature. The blackbody radiance estimation is then unfiltered with Eqs. (12) and (13). However, for a large range of T_{BBS3} between 290 and 310 K, the F_3 coefficient has been calculated from Eq. (13) and found constant with negligible variations ($\pm 1.5 \times 10^{-3}$) that require no further spectral correction of the blackbody radiance observed in the calibration mode.

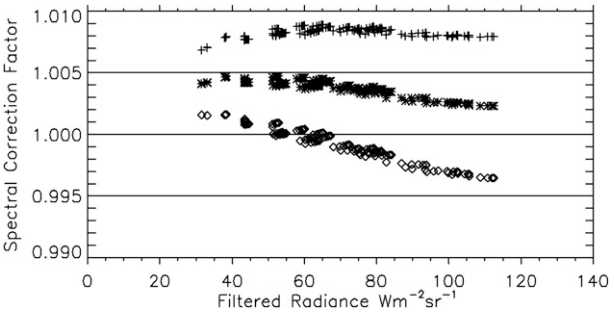

FIG. 7. LW spectral correction and impact of uncertainties beyond 20 μm. The median points (asterisk) correspond to the nominal value of the spectral response shown in Fig. 3. The impact of a progressive error starting at 20 μm and reaching 15% at 100 μm is shown by the other packets (cross and diamond).

3) LW SPECTRAL CORRECTION

When the instrument observes the earth, an equation equivalent to (13) defines the filtering factor, with the spectral radiance of the scene $L_{scene}(\lambda)$ replacing the blackbody radiance $L_{BBS3}(\lambda, T_{BBS3})$. Figure 7 shows the variations of the filtering factor F_{scene} for a large variety of terrestrial scenes. The spectral radiance dataset is based on the 168 spectra computed with Moderate Resolution Transmittance Code 6 (LOWTRAN 6; Kneizys et al. 1983) and used in a previous study (Viollier et al. 1995). New spectra are added from computations with Santa Barbara Disort Atmospheric Radiative Transfer (SBDART; Ricchiazzi et al. 1998). In Fig. 7, the median points (asterisk) correspond to the nominal values of $r_3(\lambda)$ shown in Figs. 3 and 4. Because the estimation of $r_3(\lambda)$ is not so accurate at large wavelengths, the impact of a progressive error starting at 20 μm and reaching 15% at 100 μm has also been studied and shown by the other packets (cross and diamond). This figure leads to two conclusions. First, for a given spectrum, the correction varies slowly over a range smaller than 4×10^{-3}. The almost monotonous variation as a function of radiance suggests correction at the 10^{-3} level. Second, the spectral corrections are relatively sensitive ($\pm 5 \times 10^{-3}$) to possible errors in the determination of $r_3(\lambda)$ in the domain 20–100 μm. Because the aim is an accuracy of 10×10^{-3}, this point has to be considered. This will be done during the ground calibration operations, where the $r_3(\lambda)$ values could still be evaluated and corrected. Indeed, any departure from theoretical calibrations in the response to blackbodies at different temperatures may suggest errors in $r_3(\lambda)$. This outlines the absolute need of accurate estimation of $r_3(\lambda)$ in the full spectral domain for similar future missions.

d. SW radiance

In the following, channel 2 without SW filter will be called simply channel 2, and channel 2 with SW filter will be called channel SW. The subscripts 2 and SW will be used for the corresponding parameters [$r_2(\lambda)$ and $r_{SW}(\lambda)$].

1) CALIBRATION OF CHANNEL 2 WITH NO SW FILTER

Through the C mode, channel 2 has no SW filter and observes the blackbody simulator BBS2 of the CALM at a temperature of the blackbody T_{BBS2} (normally close to T_{BBS3}). By replacing subscript 3 by 2, all the equations and the rationale of the preceding section then remain valid.

Therefore, gain G_2 is computed as

$$G_2 = \frac{N_2}{L^f_{BBS2}}, \quad \text{with} \tag{14}$$

$$L^f_{BBS2} = L_{BBS2} F_2(T_{BBS2}) \quad \text{and} \tag{15}$$

$$F_2(T_{BBS2}) = \frac{\int_0^\infty L_{BBS2}(\lambda, T_{BBS2}) r_2(\lambda)\, d\lambda}{\int_0^\infty L_{BBS2}(\lambda, T_{BBS2})\, d\lambda}. \tag{16}$$

The gains G_2 and G_3 nominally are close together, but they also may be slightly different because of the detection chain (detector, amplifier, etc). The spectral responses $r_2(\lambda)$ and $r_3(\lambda)$ are close to each other, so F_2 and F_3 should be quasi-identical, close to 1, and with negligible variations [see section 5c(2)].

2) TRANSFER FOR SW MEASUREMENTS

In the measurement mode (Fig. 2, nominal mode), channel 2 is covered by the SW filter of the filter wheel. This filter has an absolute mean transmittance T_{filter} (estimated to be 0.931 according to section 4b) and an absolute spectral transmittance $t_{filter}(\lambda)$ shown in Fig. 5. The SW spectral response is then written as

$$r_{sw}(\lambda) = r_2(\lambda) t_{filter}(\lambda). \tag{17}$$

When looking at the earth, according to the gain definition, the filtered SW radiance of the scene is given by

$$L^f_{sceneSW} = \frac{N_2}{G_2}, \tag{18}$$

no matter if the incoming radiance is SW (earth view) or LW (C-mode calibration).

In these conditions, the filtered radiance $L^f_{sceneSW}$ is defined as

$$L^f_{sceneSW} = \int_0^\infty L_{sceneSW}(\lambda) r_2(\lambda) t_{filter}(\lambda)\, d\lambda, \tag{19}$$

which can be approximated as

$$L^f_{sceneSW} = T_{filter} \int_0^\infty L_{sceneSW}(\lambda) r_2(\lambda)\, d\lambda \tag{20}$$

if T_{filter}, mean transmittance, is considered as a constant ($\sim$0.931) in the spectral range where the SW radiance is significant. As a result, the decrease of the incoming radiance by the filter transmission will be taken into account in the computation of $L^f_{sceneSW}$ and then in the filtering factors at the level-2 processing. The transfer of the T calibration to the SW domain is the combination of Eqs. (3), (4), and (19) summarized in

$$L_{SW} = \frac{N_2}{G_2} \frac{\int_0^\infty L_{scene}(\lambda)\, d\lambda}{\int_0^\infty L_{scene}(\lambda) r_2(\lambda) t_{filter}(\lambda)\, d\lambda}. \tag{21}$$

In conclusion, as for channel 3, the gain G_2 is directly calculated within the C mode using Eq. (18), with the filtering factor [Eqs. (15) and (16)] and L_{BBS2} calculated from the Stefan–Boltzmann constant and the measured temperature T_{BBS2}. The influence of the silica filter used in the measurement mode is taken into account in the definition of the filtered radiance [Eq. (19)] and then removed when the unfiltered radiances are calculated at level 2 [Eq. (21)].

3) SW SPECTRAL CORRECTIONS

Equation (21) includes the SW filtering factor [Eq. (4)] calculated with r_{sw} [Eq. (17)]. As seen in these equations, the filtering factor F_{scene} depends on $L_{scene}(\lambda)$ (i.e., on the scene color). To simulate a large variety of $L_{scene}(\lambda)$, we use the same set of 680 radiance spectra as in a previous study (Viollier et al. 1995), computed with the Simulation of a Satellite Signal in the Solar Spectrum (5S; Tanré et al. 1990) for the SW domain over clear-sky scenes and Global Atmosphere Model (GAME; Dubuisson et al. 1996, 2004) over different cloudy scene types.

For clear atmosphere targets and for the shortwave domain, the 5S model is used, because it takes into account atmospheric absorption and scattering effects. Four types of scene have been considered: vegetation, sand, ocean with clear atmosphere (23-km visibility), and ocean with haze (5-km visibility). For each scene, there are 11 cases relative to various viewing geometries, water vapor, and ozone content. These SW signatures have been computed from 0.25 to 2.2 μm with 5-nm

resolution. Spectral signatures of cloudy scenes for the SW domain were simulated by the radiative transfer code GAME (Dubuisson et al. 1996, 2004), which is based on the discrete ordinate method. This code calculates the radiances reflected by a vertically inhomogeneous scattering atmosphere and takes into account various atmospheric parameters: ozone, water vapor, aerosols, surface albedo, droplet size, altitude, and optical depth of clouds.

Filtering factors are computed from Eq. (4), and the comparison between ERB instruments is shown in Table 2. For making significant the comparisons, all the spectral responses have been normalized in the same way (filtering factor equal to 1 for a blackbody at 5800 K). The largest errors are found for CERES/Tropical Rainfall Measuring Mission (TRMM) and GERB-2 with a simple explanation: the cutoff between 0.3 and 0.4 μm, which neglects a significant part of the reflected solar radiation, specifically on clear-sky scenes. Indeed, the error rapidly grows from a cutoff between 0.325 and 3.50 μm (between 0.15% and 1.25%). On the contrary, small errors are found for the ScaRaB instrument that take advantage of its telescope with only one mirror. In the ScaRaB series, the smallest error is found for ScaRaB-3. This last result cannot be fully explained, because it results from the complex convolution of the spectral response with variable scene spectral signatures. The ScaRaB-3 spectral response is slightly different from those of ScaRaB-1 and ScaRaB-2, probably because of small differences in the production of the mirrors. In Fig. 6, the spectral response seems flatter for ScaRaB-2 than for ScaRaB-3 between 0.4 and 0.9 μm. However, if we extend the interval to 1.2 μm, the variation is overall smaller for ScaRaB-3, which explains the low level of spectral correction found in Table 2.

In conclusion, the filtered radiance is converted to real radiance using Eq. (3) and the value of the filtering factor F_{scene}. The range of variation for F_{scene} and for the corresponding spectral errors (Table 2) is particularly small for ScaRaB-3. Indeed, the SW spectral response is not particularly flat, but it covers rather uniformly the full SW domain. Although the resulting ScaRaB-3 rms errors is small (0.6 W m^{-2}) and the spectral corrections can be omitted, we still will try to reduce this error by searching for correction function of the scene type.

e. Daytime LW

We recall that the LW radiance for daytime is deduced from the difference between the total and SW channels. According to the general definition [Eq. (1)], the resulting difference corresponds to the LW filtered radiance

$$L^f_{\text{LW}} = \int_0^\infty L_{\text{LW}}(\lambda) r_3(\lambda)\, d\lambda, \tag{22}$$

which can be written as

$$L^f_{\text{LW}} = \int_0^\infty L_{\text{T}}(\lambda) r_3(\lambda)\, d\lambda - \int_0^\infty L_{\text{SW}}(\lambda) r_3(\lambda)\, d\lambda. \tag{23}$$

The SW radiation is included in both SW and total measurement and filtered by $r_{\text{sw}}(\lambda)$ and $r_3(\lambda)$, respectively. The ratio of these two filtered SW filtered values is called A', according to the symbol used earlier (Viollier et al. 1995):

$$A' = \frac{\int_0^\infty L_{\text{SW}}(\lambda)\, r_3(\lambda)\, d\lambda}{\int_0^\infty L_{\text{SW}}(\lambda)\, r_{\text{SW}}(\lambda)\, d\lambda}. \tag{24}$$

Assuming this coefficient is constant whatever the scene observed, Eq. (23) becomes

$$L^f_{\text{LW}} = L^f_{\text{T}} - A' L^f_{\text{SW}}. \tag{25}$$

The assumption that A' is constant, whatever the scene, is justified if the shape of both spectral responses is similar in the SW domain: more exactly, if the ratio $r_3(\lambda)/r_{\text{SW}}(\lambda)$ is constant when $L_{\text{sw}}(\lambda) r_{\text{SW}}(\lambda)$ is significantly different from zero. For each ScaRaB, this hypothesis has been checked with a large set of modeled earth spectral radiances. The coefficient A' was found constant ($\pm$0.3% peak to peak). Because A' is constant no matter the scene, its value can be easily computed by replacing the $L_{\text{sw}}(\lambda)$ value in Eq. (24) by the radiance of a blackbody at 5800 K (close to the solar spectrum):

$$A' = \frac{\int_0^\infty B(\lambda, 5800) r_3(\lambda)\, d\lambda}{\int_0^\infty B(\lambda, 5800) r_{\text{SW}}(\lambda)\, d\lambda}. \tag{26}$$

Here, A' was found to be equal to 0.845 and 0.895 for ScaRaB-1 and ScaRaB-2, respectively. Note that these values depend on the normalization of the spectral response (see section 5b). Under the same conditions, A' is equal to 0.910 for ScaRaB-3.

According to Eq. (25), the factor A' is also defined by

$$A' = \frac{L^f_{0\text{T}}}{L^f_{\text{SW}}}, \tag{27}$$

where $L^f_{0\text{T}}$ and L^f_{sw} are the T and SW filtered radiances when channels 2 and 3 observe a same SW source

[$L^f_{LW} = 0$ in Eq. (25)]. In that case, Eq. (27) can be written as

$$A' = \frac{AG_2}{G_3}, \tag{28}$$

where A is the ratio of numerical counts N_3/N_2 observed in this condition. Consequently, there are two methods to estimate A':

1) from the spectral responses $r_{SW}(\lambda)$ and $r_3(\lambda)$, Eq. (26); and
2) from the observation of a pure SW source by both channels, Eq. (28).

The second estimation can be obtained in flight with the S-mode calibration. To take into account the attenuation by the filter on channel 3, N_3 has then to be divided by the filter transmittance before calculating A. In conclusion, the LW daytime unfiltered radiance is obtained from the total and SW unfiltered radiances and from the A' coefficient. This last parameter is a key parameter, which requires careful assessment, specifically in the preflight calibration operations.

f. Thermal leak near 4 μm

The separation of the solar and thermal components between 3.5 and 4 μm has been studied for example for the analysis of the National Oceanic and Atmospheric Administration (NOAA) Advanced Very High Resolution Radiometer (AVHRR) SW IR channel (Trishchenko 2006) for ERB instruments, there is also a small contribution of emitted thermal radiation to the SW radiance beyond 40 μm, where the silica filter is not completely opaque. The addition of both contributions can be approximated from the relationship between the SW daytime and IR window channels (Fig. 8 for ScaRaB). During daytime, the relationship can be used to estimate and remove this SW thermal leak. Note that this contribution is very small (less than 1 W m^{-2} sr^{-1}) but not negligible for reaching the 1% accuracy goal. Direct observations from ScaRaB-2 confirm the theoretical estimations by setting the relationship between the SW daytime and IR window radiances (W m^{-2} sr^{-1}) to be

$$R_{SW}^{\text{thermal leak}} \sim 0.04\, R_{IR}. \tag{29}$$

6. Geophysical cross-calibration methods

Because the objective of 1% radiometric accuracy is so difficult to reach, cross checking with vicarious calibration methods using direct earth observations are useful and recommended. Two methods are described in this section.

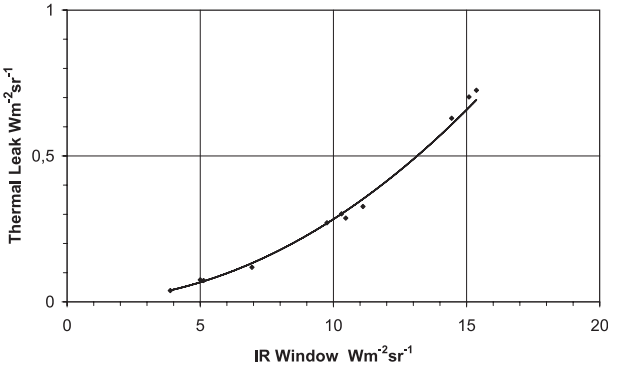

FIG. 8. Theoretical estimation of thermal leak (LW radiation encompassed in the SW signal) as a function of the nighttime infrared radiance for overcast to clear-sky conditions.

a. The three channels consistency approach

This method was developed by Duvel and Raberanto (2000) for assessing the SW response of ScaRaB and is used in the CERES processing (Priestley et al. 2000). The principle is to compare the SW radiance to the SW part of the total channel radiance. To isolate that part, the method uses the observations over DCC in the tropics. DCC are selected from cloud-top temperatures colder than 205 K. Over these clouds, very bright and cold, the SW radiance constitutes the major part of the signal. The LW radiance is small but non-negligible. It can be estimated by the IR window channel with sufficient accuracy, because the DCC altitudes are >10 km, and then both channels are very little affected by possible but small variations (mostly in the CO_2 and ozone bands) of atmospheric absorption and emission above the cloud top. This is likely, even if the pixel is not uniformly filled by DCC, because only pixels with the very low average window IR signal corresponding to 205 K are selected. Consequently, this target of spectrum covering all the solar wavelengths has a known SW radiance, without involving atmospheric modeling. It makes a perfect reference source to compute SW gain and to check the unfiltering process.

This approach when applied to ScaRaB-2 measurements gives cross-calibration parameters with accuracy better than 1%. We can summarize this approach by saying that this method transfers the reliable channel 3 calibration to the SW channel. However, the SW calibration is assessed by this method only if the SW spectral responses of the total and SW channels are well characterized and not degraded. Any change can arise from either an error in the absolute accuracy of the SW channel gain or from the SW part of the total channel.

b. The deep convective cloud as SW reference

After many theoretical and empirical studies, Hu et al. (2004) recommended to use the DCC as a substitute of the CERES SW onboard calibration source, because the lamp system is unfitted to get the filter aging (Matthews et al. 2005). Indeed, these DCC have such large optical thicknesses that they give a strong, stable, and isotropic reflection. They can be regarded as stable, because changes in the absorption by ozone are not expected in the tropics, as well as variations in size and shape of ice crystals, because the DCC crystals are composed of fresh and small crystals.

DCC are selected from cloud-top temperatures colder than 205 K. The optical depth for these clouds are most likely greater than 100. The albedo distribution is peaked at 0.76, with small variance. The albedo distribution was also demonstrated almost identical from month to month. In parallel, Hu et al. (2004) explore theoretical development to strengthen this method. These arguments have led the CERES team to progressively use the DCC as SW calibration source in place of the onboard solar diffuser (not reliable) and of the lamps (stable but not sensitive to the UV–blue spectral degradation).

7. Summary of the ScaRaB-3 calibration strategy

This paper has recalled the general principles of radiometric broadband calibration and has outlined the improvements sought for ScaRaB-3. Here is a summary of the ScaRaB-3 recommended calibration strategy for the broadband channels:

1) The nighttime LW unfiltered radiance is derived from channel 3 and calculated through gain G_3. This gain is directly estimated within the C mode from the observation of the blackbody simulator 3 and of its temperature T_{BBS3}. At level 2, radiance is unfiltered by using the filtering factor (Fig. 7) to take into account the nonflatness of the spectral response, but this spectral correction does not exceed $\pm 0.4\%$.
2) The SW radiance is derived from channel 2. Gain G_2 is calculated within the C mode exactly as the G_3 gain but using blackbody simulator 2 (then from the measured T_{BBS2} temperature instead of T_{BBS3}). The influence of the silica filter used in the measurement mode is taken into account in the definition of the filtered radiance [Eq. (19)] and in the calculation of the unfiltered radiances calculated at level 2. The small thermal leak (<2 W m^{-2} sr^{-1}) is removed from extrapolation based on the narrowband infrared channel. One of the most interesting findings is the low level of the spectral correction compared to other ERB instruments.
3) The LW daytime unfiltered radiance is obtained from the total and SW unfiltered radiances and from the A′ coefficient computed from the SW and total spectral signatures. At level 2, radiance is unfiltered by using the filtering factor (Fig. 7).
4) The key coefficient A' is checked in the S-mode calibration mode. In this mode, each main channel observes the same SW signal. Any departure of the SW response in one channel can be compared to the other and will be detected. This mode also allows checking the independence of A' with regard to the large variety of colors of earth scenes.
5) Any relative change in the LW response of each main channel can be detected in the T-mode calibration mode. In this mode, each main channel observes the total radiation from a variety of earth scenes.
6) The three-channel consistency method allows checking the G_{sw} gain, and it is complementary to the S-mode calibration mode, because it is independent of any SW filter transmittance change.
7) All the previous SW assessments are extremely useful, but they cannot detect parallel degradation of the spectral responses in both main channels. Finally, the DCC method (assuming valid the hypothesis of stable target) also checks the G_{sw} gain, including the impact of any degradation of the SW spectral response.

It is only from all these independent tests that the radiometric accuracy will be reliable and documented. Before the flight, ground calibration and tests under vacuum chamber are planned, giving the opportunity for ultimate adjustments of the radiometric and spectral characterizations before launch. This study has led to compare the SW errors resulting from spectral responses of different ERB instruments. Because of mirror characteristics, the cutoff is around 0.35 μm for CERES and GERB, a spectral region where the reflected solar radiation grows rapidly. This characteristic leads to larger errors (by a factor of 2) than those found for ScaRaB and ERBE.

Acknowledgments. The ScaRaB instruments were designed by J. L. Monge in the 1980s and checked and improved by F Sirou in the 1990s. R. Kandel and J. P. Duvel were successively the PI of the ScaRaB space missions launched in 1994 and 1998. This article then borrows many descriptions from these previous works. After five years of work, the update and production of the Optical Sensor Module (OSM) were achieved at LMD by a team of talented engineers and technicians (Christine Gasq, Daniel Sourgen, Olivier Bousquet, Gilles Bannerot, André Guilbaud, and Jacqueline Albert). They

succeeded in delivering the OSM to CNES in November 2008. Since 2004, the project is under CNES responsibility, with Nadia Karouche as Megha-Tropiques project leader, Jean François Reulet followed by Alain Rosak as ScaRaB project manager, and Thierry Trémas as responsible for the calibration and location data processing. Dr. Jacques Hameury (Laboratoire National de Métrologie et d'Essais, F78187 Trappes) and his colleagues provided spectral characteristics of filters, mirrors, and blackbodies. This article benefits also from the CERES project (notably information from Kory Priestley and Norman Loeb) and from the GERB project (information provided by Jacqueline Russell and the spectral information available online at http://ggsps.rl.ac.uk/information.html#Spectral).

Michel Viollier passed away 30 June 2009, after a long and courageous battle with cancer, during which he maintained his activity and continued to contribute to the drafting and revision of this paper.

REFERENCES

Barkstrom, B., and Coauthors, 1989: Earth Radiation Budget Experiment (ERBE) archival and April 1985 results. *Bull. Amer. Meteor. Soc.,* **70,** 1254–1262.

Bess, T. D., G. L. Smith, R. N. Green, D. A. Rutan, R. S. Kandel, P. Raberanto, and M. Viollier, 1997: Intercomparison of Scanning Radiometer for Radiation Budget (ScaRab) and Earth Radiation Budget Experiment (ERBE) results. *Proc. Ninth Conf. on Atmospheric Radiation,* Long Beach, CA, Amer. Meteor. Soc., 203–207.

Buriez, J.-C., F. Parol, Z. Poussi, and M. Viollier, 2007: An improved derivation of the top-of-atmosphere albedo from POLDER/ADEOS-2: 2. Broadband albedo. *J. Geophys. Res.,* **112,** D19201, doi:10.1029/2006JD008257.

Clerbaux, N., and Coauthors, 2008a: Unfiltering of the Geostationary Earth Radiation Budget (GERB) data. Part I: Shortwave radiation. *J. Atmos. Oceanic Technol.,* **25,** 1087–1105.

——, S. Dewitte, C. Bertrand, D. Caprion, B. De Paepe, L. Gonzalez, A. Ipe, and J. E. Russell, 2008b: Unfiltering of the Geostationary Earth Radiation Budget (GERB) data. Part II: Longwave radiation. *J. Atmos. Oceanic Technol.,* **25,** 1106–1117.

Dewitte, S., L. Gonzalez, N. Clerbaux, A. Ipe, C. Bertrand, and B. De Paepe, 2008: The Geostationary Earth Radiation Budget Edition 1 data processing algorithms. *Adv. Space Res.,* **41,** 1906–1913.

Dubuisson, P., J. C. Buriez, and Y. Fouquart, 1996: High spectral resolution solar radiative transfer in absorbing and scattering media: Application to the satellite simulation. *J. Quant. Spectrosc. Radiat. Transf.,* **55,** 103–126.

——, D. Dessailly, M. Vesperini, and R. Frouin, 2004: Water vapor retrieval over ocean using near-IR imagery. *J. Geophys. Res.,* **109,** D19106, doi:10.1029/2004JD004516.

Duvel, J. P., and P. Raberanto, 2000: A geophysical cross-calibration approach for broadband channels: Application to the ScaRaB experiment. *J. Atmos. Oceanic Technol.,* **17,** 1609–1617.

——, and Coauthors, 2001: The ScaRaB–Resurs Earth radiation budget dataset and first results. *Bull. Amer. Meteor. Soc.,* **82,** 1397–1408.

Gelsthorpe, R. V., A. Heliere, A. Lefebvre, J. Lemanczyk, E. Mateu, and K. Wallace, 2008: EarthCARE and its payload. Proc. *Remote Sensing of the Atmosphere and Clouds II,* G. L. Stephens and T. Y. Nakajima, Eds., International Society for Optical Engineering (SPIE Proceedings, Vol. 7152), 715207, doi:10.1117/12.804914.

Haeffelin, M., B. Wielicki, J. P. Duvel, K. Priestley, and M. Viollier, 2001: Inter-calibration of CERES and ScaRaB Earth Radiation Budget datasets using temporally and spatially collocated radiance measurements. *Geophys. Res. Lett.,* **28,** 167–170.

Harries, J. E., and Coauthors, 2005: The Geostationary Earth Radiation Budget project. *Bull. Amer. Meteor. Soc.,* **86,** 945–960.

Hu, Y., B. A. Wielicki, P. Yang, P. W. Stackhouse, B. Lin, and D. F. Young, 2004: Application of deep convective cloud albedo observation to satellite-based study of the terrestrial atmosphere: Monitoring the stability of spaceborne measurements and assessing absorption anomaly. *IEEE Trans. Geosci. Remote Sens.,* **42,** 2594–2599.

Kandel, R. S., J. L. Monge, M. Viollier, L. A. Pakhomov, V. I. Adasco, R. G. Reitenbach, E. Raschke, and R. Stuhlmann, 1994: The ScaRaB project: Earth radiation budget observations from the Meteor satellites. *Adv. Space Res.,* **14,** 47–54.

——, and Coauthors, 1998: The ScaRaB Earth Radiation Budget dataset. *Bull. Amer. Meteor. Soc.,* **79,** 765–783.

Kneizys, F. X., E. P. Shettle, W. O. Gallery, J. H. Chetwynd Jr., L. W. Abreu, J. E. A. Selby, S. A. Clough, and R. W. Fenn, 1983: Atmospheric transmittance/radiance: Computer code LOWTRAN 6. Air Force Geophysics Laboratory Environmental Research Paper 846, AFGL-TR-83-0187, 200 pp.

Koepke, P., 1982: Vicarious satellite calibration in the solar spectral range by means of calculated radiances and its application to Meteosat. *Appl. Opt.,* **21,** 2845–2854.

Loeb, N. G., K. J. Priestley, D. P. Kratz, E. B. Geier, R. N. Green, B. A. Wielicki, P. O. Hinton, and S. K. Nolan, 2001: Determination of unfiltered radiances from the Clouds and the Earth's Radiant Energy System instrument. *J. Appl. Meteor.,* **40,** 822–835.

——, B. A. Wielicki, D. R. Doelling, G. L. Smith, D. F. Keyes, S. Kato, N. Manalo-Smith, and T. Wong, 2009: Toward optimal closure of the earth's top-of-atmosphere radiation budget. *J. Climate,* **22,** 748–766.

Matthews, G., K. Priestley, P. Spencer, D. Cooper, and D. Walikainen, 2005: Compensation for spectral darkening of short wave optics occurring on the Cloud's and the Earth's Radiant Energy System. *Earth Observing Systems X,* J. L. Butler, Ed., International Society for Optical Engineering (SPIE Proceedings, Vol. 5882), 588212, doi:10.1117/12.618972.

Monge, J. L., R. Kandel, L. A. Pakhomov, and V. I. Adasko, 1991: ScaRaB Earth Radiation Budget scanning radiometer. *Metrologia,* **28,** 261–284.

Mueller, J., and Coauthors, 1997: Ground characterization of the Scanner for Radiation Budget (ScaRaB) flight model 1. *J. Atmos. Oceanic Technol.,* **14,** 802–813.

Priestley, K. J., and Coauthors, 2000: Postlaunch radiometric validation of the Clouds and the Earth's Radiant Energy System (CERES) proto-flight model on the Tropical Rainfall Measuring Mission (TRMM) spacecraft through 1999. *J. Appl. Meteor.,* **39,** 2249–2258.

——, B. A. Wielicki, R. N. Green, M. P. A. Haeffelin, R. B. Lee, and N. G. Loeb, 2002: Early radiometric validation results of the CERES flight model 1 and 2 instruments onboard NASA's Terra spacecraft. *Adv. Space Res.,* **30,** 2371–2376.

Ricchiazzi, P., S. Yang, C. Gautier, and D. Sowle, 1998: SBDART: A research and teaching software tool for plane-parallel radiative transfer in the Earth's atmosphere. *Bull. Amer. Meteor. Soc.,* **79,** 2101–2114.

Sirou, F. E., M. C. Dinguirard, P. Churoux, and T. Tremas, 1997: ScaRaB ground calibration. *Earth Observing Systems II,* W. L. Barnes, Ed., International Society for Optical Engineering (SPIE Proceedings, Vol. 3117), 294–305.

Tanré, D., C. Deroo, P. Duhaut, M. Herman, J. J. Morcrette, J. Perbos, and P. Y. Deschamps, 1990: Description of a computer code to simulate the satellite signal in the solar spectrum: The 5S code. *Int. J. Remote Sens.,* **11,** 659–668.

Trémas, T., and M. Dinguirard, 1997: Calibration of ScaRaB FM1: Methods and first results. *Adv. Space Res.,* **19,** 1335–1343.

Trishchenko, A. P., 2006: Solar irradiance and effective brightness temperature for SWIR channels of AVHRR/NOAA and GOES imagers. *J. Atmos. Oceanic Technol.,* **23,** 198–210.

Viollier, M., 1982: Radiometric calibration of the Coastal Zone Color Scanner on Nimbus 7: A proposed adjustment. *Appl. Opt.,* **21,** 1142–1145.

——, R. Kandel, and P. Raberanto, 1995: Inversion and space-time averaging algorithms for ScaRaB (Scanner for Earth Radiation Budget)—Comparison with ERBE. *Ann. Geophys.,* **13,** 959–968.

Wielicki, B. A., B. R. Barkstrom, E. F. Harrison, R. B. Lee III, G. Louis Smith, and J. E. Cooper, 1996: Clouds and the Earth's Radiant Energy System (CERES): An Earth Observing System experiment. *Bull. Amer. Meteor. Soc.,* **77,** 853–868.